J. Phys. Chem. A **2006,** *110,* 5317−5325

Assignment and Extraction of Dynamics of a Small Molecule with a Complex Vibrational Spectrum: Thiophosgene[†]

Christof Jung

Centro de Ciencias Físicas, Universidad Nacional Autónoma de México, Av. Universidad s/n, 62251 Cuernavaca, México

Howard S. Taylor

Department of Chemistry, University of Southern California, Los Angeles, California 90089

Edwin L. Sibert III*

Department of Chemistry and Theoretical Chemistry Institute, University of Wisconsin Madison, Madison, Wisconsin 53706

Received: October 5, 2005; In Final Form: November 29, 2005

The dispersed fluoresence spectrum of the ground electronic state of thiophosgene, $SCCl_2$, is analyzed in a very complex region of vibrational excitation, 7000−9000 cm^{-1}. The final result is that most of the inferred excited vibrational levels are assigned in terms of approximate constants of the motion. Furthermore, each level is associated with a rung on a ladder of quantum states on the basis of common reduced dimension fundamental motions. The resulting ladders cannot be identified by any experimental means, and it is the interspersing in energy of their rungs that makes the spectrum complex even after the process of level separation into polyads. Van Vleck perturbation theory is used to create polyad constants of the motion and a spectroscopic Hamiltonian from a potential fitted to experimental data. The eigenfuntions of this spectroscopic Hamiltonian are rewritten as semiclassical wave functions and transformed to a representation that allows us to analyze and assign the spectra with no other work other than to utilize concepts from nonlinear dynamics.

I. Introduction

Bigwood et al.[1] experimentally determined the dispersed fluoresence spectrum of $SCCl_2$, probing the zero to 15 000 cm^{-1} wavenumber vibrational excitation spectral region. About half of the 200 observed transitions were either assigned or fit, the great majority of these transitions occurring below 7000 cm^{-1}. Above this energy, and in particular in the energy regime from 7000 to 9000 cm^{-1}, the spectrum is quite complex, and conventional interpretative methods[2] failed in the sense of assigning quantum numbers, which are quasiconstants of the motion, in the amount needed for the six degrees of freedom system. Moreover, the vibrational motions underlying the spectrum were unable to be revealed. A goal that was achieved was to use the assigned transitions to fit the spectral data to a functional form representing a parametric potential hypersurface. Bigwood et al.[1] then used this hypersurface to propagate select zero-order states at energies near 9000 cm^{-1} to aid in the interpretation of the intramolecular vibrational redistribution of energy.

Although one can use a potential energy surface in conjunction with quantum chemistry to supply wave functions or propagated wave packets to interpret spectra, the effort to make such detailed calculations for all but a few states in six degrees of freedom is prohibitive, especially in light of the high density of vibrational levels in the region of interest. Additionally, there is the certainty that these wave functions would be generically so complex as to not show the nodal patterns needed for assignment and to not allow any sorting into ladders of states based on a common dynamics. Even without the generic complexity the existence of six degrees of freedom belies the ability of the wave function to be viewed for purposes of interpretation.

Faced with these complexities, researchers, exploiting the classical-quantum correspondence principle, have had great success using classical mechanics to gain novel insights into the nature of eigenstates in energy regimes that are valid beyond the normal mode limit.[3−10] The key idea is that knowledge of the topology of the underlying classical phase space elucidates both eigenvalue patterns and eigenstate structures. Periodic orbits,[3,4,9] homoclinic oscillations,[10] and bifurcations[3,4,7,8] have all proven to be invaluable concepts for interpreting molecular spectra. In addition, there are often mulitiple constants of motion, acetylene[11−14] and water[3,7,15] being two excellent examples, that can be utilized to further simplify the analysis of the spectra. One advantage of these constants is that the classical dynamics can be visualized in a reduced dimensional space.[3]

Our work is distinct from those studies. We carry out a semiclassical analysis of the quantum wave functions in a representation that allows us to use the classical-quantum correspondence principle to assign our spectra in a manner that is consistent with common phase space structures such as stable periodic orbits and zones of nonlinear resonance.[16] As such, no classical trajectory results are needed in our analysis.

We take as our starting point the Van Vleck perturbative method[13,17−20] which we use to create an effective Hamiltonian. This block-diagonal, multiresonant spectroscopic Hamiltonian

---

[†] Part of the special issue “John C. Light Festschrift”.

10.1021/jp055679d CCC: $33.50

can then be diagonalized to determine the eigenstate wave functions in the number representation for each of the blocks, the blocks being defined by the polyad quantum numbers. In contrast to that approach, here we transform the Hamiltonian to the corresponding action-angle representation. The beauty of the action-angle representation is that it allows one to reduce effectively the dimension of the Hamiltonian by transforming to a new set of angle variables, where the transformed Hamiltonian only depends on a subset of the new angle variables. Quantization of this Hamiltonian and its subsequent eigenstate analysis allows us to visualize the wave functions and clarify which of the myriad of possible resonant interactions are important. Here all but the simplest of computations cease to be used, and our semiclassical analysis is employed to assign states.

The semiclassical analysis was developed in previous studies of complex vibrations for such molecules as acetylene,[13,14] CHBrClF,[21] N_2O,[22] DCO,[23] CDBrClF,[24] and CF_3CHFI.[25] The analysis allows inspection of the density and phases of its eigenfunctions previously calculated in the Hamiltonian derivation process but now transformed to a reduced dimension semiclassical action-angle representation. This reveals extremely simple albeit unfamiliar topologies that give quantum numbers by simply counting nodes and phase advances.

The topology also allows us to sort most states, even though they have unfamiliar forms, into dynamically different excitation ladders of states. Here these ladders are associated with different regions of phase space. The rungs of these ladders intersperse in energy causing the spectral complexity. No experimental procedure allows such a sorting. To demonstrate the power of this approach, we will analyze in detail a specific polyad of states whose energies are approximately 8000 cm^{-1} and which seem to form some of the most complex spectral line patterns that we have studied.

Even in classically chaotic regions guiding spinal points, trajectories, or planes that correspond to averages over regional periodic orbits can easily be drawn from these eigenfunctions as the structure about which localization takes place. The guiding dynamic elements when transformed back to the full dimensional configuration space reveal the internal molecular motions.

The spectroscopic model Hamiltonian results are sensitive to model changes in the potential. This coupled with the fact that our analysis is based on second-order perturbation theory, should lead one to expect the eigenvectors to be qualitative. This is correct. Nonetheless, much of the interesting topologies found here are robust to modest potential changes and to the order of perturbation theory, even though the details of the interleaving of the rungs of the ladder will certainly change. From our perspective, the important issue is to demonstrate the utility of the approach for analyzing wave functions of a multiresonant Hamiltonian in a strongly mixed regime where traditional methods fail entirely. The sensitivity presents no problem for the purpose of sorting assigning and extracting dynamics.

II. Van Vleck Perturbative Results

We have chosen the rectilinear normal mode Hamiltonian as our starting point for the calculation of the effective Hamiltonian. For $SCCl_2$ this Hamiltonian takes the simple form

$$H_v = \frac{1}{2}\sum_k P_k{}^2 + V(\boldsymbol{Q}) \tag{1}$$

where the small inverse moment of inertia terms are neglected.

TABLE 1: Calculated Normal Mode Frequencies (cm^{-1})

mode	symmetry	$\tilde{\omega}_i$	description
1	a_1	1153.26	S═C stretch
2	a_1	507.51	C−Cl stretch
3	a_1	290.60	Cl−C−Cl bend
4	b_1	470.30	out-of-plane
5	b_2	845.85	C−Cl stretch
6	b_2	329.20	Cl−C−Cl bend

The potential is that of Strickler and Gruebele,[26] this potential being similar to that of Bigwood et al.[1] Following Nielsen,[17] we expand the Hamiltonian in the form

$$H_v = H_v^{(0)} + \lambda H_v^{(1)} + \lambda^2 H_v^{(2)} + \cdots + \lambda^n H_v^{(n)} \tag{2}$$

where λ is the perturbation parameter. The potential terms of order n are included in $H_v^{(n-2)}$. This Hamiltonian is reexpressed in terms of harmonic oscillator raising and lowering operators.

The Van Vleck transformations are accomplished via a succession of canonical transformations,

$$K_v = T^{(n)} \cdots T^{(2)} T^{(1)} H_v \tag{3}$$

where $T^{(n)} = \exp\{i\lambda^n[S^{(n)},\ ]\}$. The $S^{(n)}$ are chosen such that

$$\hat{K}_v = \sum_{\{\vec{m},\vec{n}\}} c_{\vec{m},\vec{n}} \prod_{i=1}^{6} [(a_i^\dagger)^{m_i} a_i^{n_i}] \tag{4}$$

has the desired form through order n.[18] This transformed Hamiltonian is written in terms of raising and lowering operators that obey the same commutation relations, e.g., $[a, a^\dagger] = 1$, as those for the harmonic oscillator. Both H_v and K_v have zero-order contributions that describe uncoupled harmonic oscillators, whose descriptions are given in Table 1.

There are many different forms K_v can take.[19] Given the normal-mode frequencies we have chosen the $S^{(n)}$ such that each of the following operators

$$\begin{aligned} \hat{K} &= \hat{v}_1 + \hat{v}_2 + \hat{v}_5 \\ \hat{L} &= 2\hat{v}_1 + \hat{v}_3 + \hat{v}_5 + \hat{v}_6 \\ \hat{M} &= \hat{v}_4 \end{aligned} \tag{5}$$

commute with the Hamiltonian $\hat{K}_v$ when off-diagonal terms greater than order n are neglected. Here $\hat{v}_i = a_i^\dagger a_i$ is the number operator. Equivalently, the $S^{(n)}$ are chosen such that the matrix representation of K_v is block-diagonal. These operators are found by examining the normal-mode frequencies and determining which sets of states are likely to be resonantly coupled. With this information one finds the above operators using an algorithm such as the Kellman vector model.[11] It should be noted that although any three independent combinations of these operators can be used, we found the above choice of operators to be the most convenient. It should also be noted that the number of additional constants depends entirely on the symmetry, the couplings, zero-order normal-mode frequencies, and the energy range over which one hopes to carry out the analysis.

The final Hamiltonian takes the form of harmonic oscillators plus anharmonic corrections

$$K_v = \sum_i^6 \tilde{\omega}_i\left(\hat{v}_i + \frac{1}{2}\right) + \sum_{i \le j} x_{ij}\left(\hat{v}_i + \frac{1}{2}\right)\left(\hat{v}_j + \frac{1}{2}\right) + W_{qm} \tag{6}$$

TABLE 2: Calculated x_{ij} (cm^{-1}) from Second-Order Perturbation Theory

$i\ j$	x_{ij}	$i\ j$	x_{ij}
1 1	−3.149392	2 5	−4.502738
1 2	0.248292	3 5	−1.788787
2 2	−1.101397	4 5	−3.165362
1 3	0.069427	5 5	−4.848639
2 3	−1.230195	1 6	−1.489753
3 3	−0.160529	2 6	−0.307362
1 4	−2.093491	3 6	0.048541
2 4	−2.737102	4 6	−3.861793
3 4	−2.161802	5 6	−1.703855
4 4	2.302492	6 6	−0.325367
1 5	−4.464485		

TABLE 3: Off-Diagonal Coupling Terms (cm^{-1}) through Second-Order Perturbation Theory Written in the Form of Eq 4[a]

coeff	$c_{m,n}$	m						n					
k_{156}	−10.0317	0	0	0	0	1	1	1	0	0	0	0	0
k_{526}	−10.8573	0	0	0	0	1	0	0	1	0	0	0	1
k_{231}	0.0491	0	1	2	0	0	0	1	0	0	0	0	0
k_{261}	−0.0452	0	1	0	0	0	2	1	0	0	0	0	0
k_{125}	4.1329	1	1	0	0	0	0	0	0	0	0	2	0
k_{36}	−0.8228	0	0	2	0	0	0	0	0	0	0	0	2

[a] The coupling W_{qm} includes the hermitian conjugates of these terms.

The x_{ij} are given in Table 2 and the off-diagonal contribution W_{qm} is given in Table 3. The first two contributions of Table 3 appear at first order in perturbation theory. They are

$$W_{qm}^{(1)} = k_{156}(a_1^\dagger a_5 a_6 + \mathrm{hc}) + k_{526}(a_5^\dagger a_2 a_6 + \mathrm{hc}) \tag{7}$$

The eigenstates are linear combinations of the number basis states. These in turn are eigenstates of the first terms in eq 6 and, of course, are separable.

The goal of this paper is to use semiclassical ideas to understand the shapes of the eigenfunctions of the above Hamiltonian. Although the eigenfunctions of the original Hamiltonian and the effective Hamiltonian will be different, if in both cases we assume that the raising and lowering operators are those for harmonic oscillators, the differences are generally small. The general shape and nodal structure is always the same. The work of Zúñiga provides a clear example.[20] The need for such a semiclassical analysis can be seen using a simple illustrative example.

The illustrative example is that which is obtained if all the off-diagonal terms are set to zero with the exception of the k_{156} term. The corresponding classical Hamiltonian is trivially integrable yet the resulting eigenstates are strongly mixed in three degrees of freedom. The k_{156} terms mixes the six zero-order number basis states $|5 - p, 2, 2, 0, 0 + p, 2 + p\rangle$ where $p = 0-5$. Figure 1 shows the highest energy eigenstate obtained from diagonalizing the corresponding 6 × 6 matrix.

In the next section we will describe our methods for choosing new semiclassical wave functions for interpreting the dynamics. This method removes all the cyclic coordinates in the classical Hamiltonian and thus leads to greatly simplified wave functions. We will see that Figure 1 will simplify to probability distribution shown in Figure 2. The coupling leads to a localized wave function along an appropriately chosen coordinate that describes a special phase relation between the three oscillators. We now turn to a discussion of the transformations needed to define such coordinates.

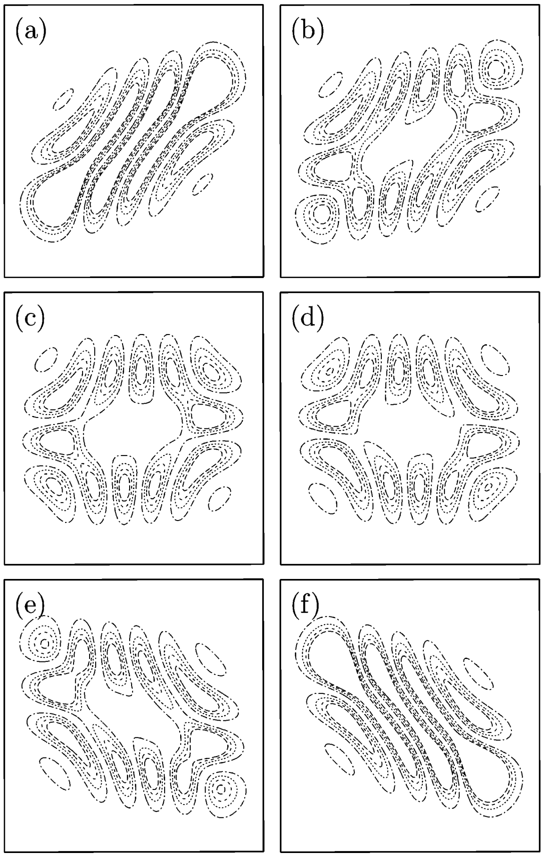

Figure 1. Probability distribution plotted as a function of the Q_5 and Q_6 coordinates for increasing values of Q_1 going from (a)−(f). This state is the highest energy state obtained from diagonalizing the Hamiltonian with all off-diagonal coupling set to zero except the k_{156} term. The k_{156} term mixes the zero-order states $|5 - p, 2, 2, 0, 0 + p, 2 + p\rangle$ where $p = 0-5$.

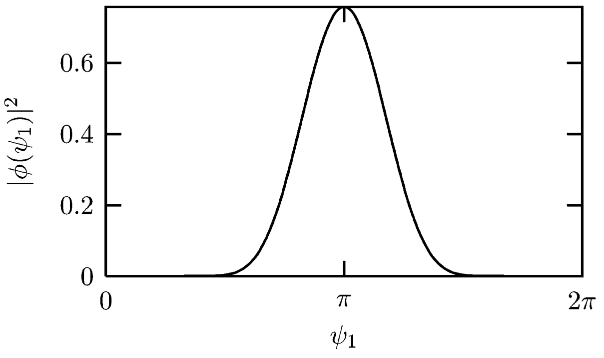

Figure 2. Semiclassical probability distribution function corresponding to that of Figure 1 plotted as a function of ψ_1 defined in eq 16.

III. Reduction and Semiclassical Wave Functions

The transition from the quantum Hamiltonian given in eq 6 in terms of creation and destruction operators to the corresponding classical Hamiltonian is done by first bringing the operators into symmetric order and then applying the semiclassical substitution rules[27]

$$a_j \rightarrow I_j^{1/2} \exp(-\mathrm{i}\phi_j) \qquad a_j^\dagger \rightarrow I_j^{1/2} \exp(\mathrm{i}\phi_j) \tag{8}$$

where I_j and ϕ_j are the classical action and angle variables for the degree of freedom j. By symmetrization we mean that we write a product of an annihilation operator with a creation operator of the same degree of freedom as $(aa^\dagger + a^\dagger a)/2$ and then the number operator transforms into classical action minus $^1/_2$. The resulting classical Hamiltonian is

$$H_{\mathrm{cl}} = H_{\mathrm{cl},0} + W_{\mathrm{cl}} \tag{9}$$

with

$$H_{\mathrm{cl},0} = \sum_j \omega_j I_j + \sum_{j \le k} x_{jk} I_j I_k \tag{10}$$

and

$$\begin{aligned} W_{\mathrm{cl}} = {} & 2k_{156} I_1^{1/2} I_5^{1/2} I_6^{1/2} \cos(\phi_1 - \phi_5 - \phi_6) + \\ & 2k_{526} I_5^{1/2} I_2^{1/2} I_6^{1/2} \cos(\phi_5 - \phi_2 - \phi_6) + \\ & 2k_{231} I_1^{1/2} I_2^{1/2} I_3 \cos(\phi_1 - \phi_2 - 2\phi_3) + \\ & 2k_{261} I_1^{1/2} I_2^{1/2} I_6 \cos(\phi_1 - \phi_2 - 2\phi_6) + \\ & 2k_{125} I_1^{1/2} I_2^{1/2} I_5 \cos(\phi_1 + \phi_2 - 2\phi_5) + \\ & 2k_{36} I_3 I_6 \cos(2\phi_3 - 2\phi_6) \end{aligned} \tag{11}$$

where the coefficients of W_{cl} are given in Table 3. The first two terms in W_{cl} correspond to those in $W_{qm}^{(1)}$ of eq 7.

In analogy to the constants of motion given in eq 5 of the quantum Hamiltonian, the classical Hamiltonian has three conserved quantities. They are

$$K = I_1 + I_2 + I_5 \tag{12}$$

$$L = 2I_1 + I_3 + I_5 + I_6 \tag{13}$$

$$M = I_4 \tag{14}$$

Be aware that the numerical values of the classical conserved quantities differ from the corresponding quantum conserved quantities because of the classical zero points of action. The quantum ground state corresponds to a value $^1/_2$ for all the classical actions of the elementary degrees of freedom.

Next we use the conserved quantities to reduce the system to one with three degrees of freedom. We apply a canonical transformation from the variables I_j and ϕ_j, $j = 1-6$ to the new actions J_1, J_2, J_3, M, K, L and canonically conjugate angles ψ_j, $j = 1-6$. To make the interpretation of the new actions easy, we choose $J_j = I_j$ for $j = 1, 2, 3$. In addition, we choose the new angles ψ_1, ψ_2 and ψ_3 as such combinations of the old angles that always move slowly and come to a complete stop in the case of frequency coupling by the resonant interactions. One possible choice with these favorable properties is

$$\begin{gathered} I_1 = J_1 \qquad I_2 = J_2 \qquad I_3 = J_3 \qquad I_4 = M \\ I_5 = K - J_1 - J_2 \qquad I_6 = L - K - J_1 + J_2 - J_3 \end{gathered} \tag{15}$$

$$\begin{gathered} \phi_1 = \psi_1 + \psi_5 + 2\psi_6 \qquad \phi_2 = \psi_2 + \psi_5 \qquad \phi_3 = \psi_3 + \psi_6 \\ \phi_4 = \psi_4 \qquad \phi_5 = \psi_5 + \psi_6 \qquad \phi_6 = \psi_6 \end{gathered} \tag{16}$$

By transforming the classical Hamiltonian of eq 9 to these new coordinates and momenta one finds that the coupling is not a function of the angles ψ_4, ψ_5, ψ_6. This is readily seen if we focus on just the coordinate dependence of the coupling which is

$$\begin{aligned} W_{cl} = {} & 2k_{156} I_1^{1/2} I_5^{1/2} I_6^{1/2} \cos(\psi_1) + \\ & 2k_{526} I_5^{1/2} I_2^{1/2} I_6^{1/2} \cos(\psi_2) + \\ & 2k_{231} I_1^{1/2} I_2^{1/2} I_3 \cos(\psi_1 - \psi_2 - 2\psi_3) + \\ & 2k_{261} I_1^{1/2} I_2^{1/2} I_6 \cos(\psi_1 - \psi_2) + \\ & 2k_{125} I_1^{1/2} I_2^{1/2} I_5 \cos(\psi_1 + \psi_2) + \\ & 2k_{36} I_3 I_6 \cos(2\psi_3) \end{aligned} \tag{17}$$

Moreover, by solving for ψ_1, ψ_2 and ψ_3 and taking the time derivative of the result to give the effective frequencies $\omega_k(J)$, here just written as ω_k, we observe that $\dot{\psi}_1$, $\dot{\psi}_2$ and $\dot{\psi}_3$ are zero when $\omega_1 = \omega_5 + \omega_6$, $\omega_2 = \omega_5 - \omega_6$ and $\omega_3 = \omega_6$, respectively. Hence as said above, the transformation is chosen to make the new variables move slowly and come to a complete stop in the case of frequency coupling by the most important (see Table 3) resonant interactions. As will be seen, such localizations will result in semiclassical wave functions being localized in the same direction. This will allow the recognition that this wave function is affected by the given resonance. It will also help in the sorting of such wave functions in classes affected by particular resonances.

As a result of the form of eq 17 the corresponding conjugate actions M, K, L can be treated as if they were parameters, and thereby the system is reduced to one with three degrees of freedom. The configuration space of the reduced system is the torus T^3 of the angle variables ψ_1, ψ_2, ψ_3. The cyclic angles conjugate to the constants of the motion have been removed.

The final goal of our whole strategy is to connect individual quantum states with some particular motion of the atoms described in the original normal coordinates of the original Hamiltonian. A necessary first step is to relate quantum states with the classical reduced configuration space T^3. In other words, we must use this T^3 as the domain on which the quantum wave functions are constructed and plotted. Taking the eigenstates as the column vectors coming out of the diagonalization of the effective Hamiltonian matrix, the conversion into a function on T^3 requires two steps. The first one is to construct the wave function as a function of angle coordinates, and the second is a reduction of the quantum system to one of three degrees of freedom in analogy to the classical reduction. We do not have any exact method for carrying out the first step. However, because all our explanations rely heavily on semiclassical thinking, it is sufficient to construct semiclassical wave functions; this can be done with amazingly little numerical effort.

We represent and replace the number states indexed by n, i.e., the basis states in which the Hamiltonian matrix is given and the eigenfunctions are represented, by the periodic plane waves on the angle torus as

$$\chi_n(\phi) = \exp\{in\phi\} \tag{18}$$

This too is the semiclassical eigenfunction of the Hamiltonian in eq 10. Here the quantities n and ϕ without any index are 6 component vectors, and in the argument of the exp function we have the scalar product of these vectors. Note that this equation corresponds to applying Schrödinger's quantization rule to the action and angle variables of the system. Of course, this only holds semiclassically because Schrödinger's rule is only valid to the lowest two orders in $\hbar$ in general canonical coordinates. Now the expansion of an eigenstate of H into number states as it comes out of the numerical diagonalization translates into the expansion of the wave function into periodic plane waves on the configuration torus. That is it translates into the Fourier decomposition of the wave function on the torus.

Next we reduce the dimensionality of the basis functions and thereby also all linear combinations of them as for example the eigenfunctions to functions of the three angle variables ψ_1, ψ_2, ψ_3. First we plug into eq 18 the expression of the old angles ϕ_j in terms of the new angles ψ_j as given in eq 16. In the argument of the exp function we obtain

$$n\phi = n_1\phi_1 + n_2\phi_2 + n_3\phi_3 + n_4\phi_4 + n_5\phi_5 + n_6\phi_6 = n_1(\psi_1 + \psi_5 + 2\psi_6) + n_2(\psi_2 + \psi_5) + n_3(\psi_3 + \psi_6) + n_4\psi_4 + n_5(\psi_5 + \psi_6) + n_6\psi_6 = \psi_1 n_1 + \psi_2 n_2 + \psi_3 n_3 + \psi_4 M + \psi_5 K + \psi_6 L \quad (19)$$

Now any eigenfunction only contains contributions from basis functions belonging to one polyad, i.e., to one value of all the conserved quantities K, L, M (here considered as combinations of the quantum excitation numbers of the original degrees of freedom). Therefore the dependence on the angles ψ_4, ψ_5 and ψ_6 is a common phase factor of all basis function and therefore a phase factor in front of the whole eigenfunction. Such global phase factors are irrelevant and can be dropped and thereby the eigenfunctions are reduced to functions of the three angle variables ψ_1, ψ_2 and ψ_3; i.e., they have become functions on the reduced classical configuration space T^3.

In summary, the basis state with excitation numbers n_j, $j = 1, ..., 6$ will be denoted by

$$|n_1, n_2, n_3\rangle \quad (20)$$

where we suppress the K, L, and M quantum numbers to simplify notation. Note that it is not necessary to specify the values of n_4, n_5, n_6, they can be reconstructed from the knowledge of the conserved quantities K, L, M. If an eigenfunction comes out of the diagonalization of the **H** matrix as a linear combination

$$|\chi_k\rangle = \sum_{n\in\text{polyad}} c_{k,n}|n\rangle \quad (21)$$

of basis functions, then the corresponding semiclassical wave function on T^3 is given as

$$\chi_k(\psi_1,\psi_2,\psi_3) = \sum_{n\in\text{polyad}} c_{k,n} \exp\{\mathrm{i}[n_1\psi_1 + n_2\psi_2 + n_3\psi_3]\} \quad (22)$$

We imagine representing the torus T^3 as a cube with identified opposite boundary points. A point on any of the cubes boundaries corresponds to one in a similar position on the opposite boundary. This is just the 3-dimensional generalization of a point on a rolling circle being able to be represented on a graph with angle varying from 0 to 2π but with enforced periodic boundary conditions. A 3-dimensional torus T^3 is a Cartesian product of three rings, thereby implying a cube with identified opposite boundary conditions. In the numerical examples in the next section we plot density (magnitude squared) and phase of some eigenfunctions on 2-dimensional sections of this cube. Also on such 2-dimensional sections opposite boundary points have to be identified such that the topology of the sections becomes the one of a 2-dimensional torus. Unfortunately, 3-dimensional perspective plots are too confusing to be useful.

The states of the quantum Hamiltonian have A_1 and B_2 symmetries. In the interaction part of the quantum Hamiltonian this is evident in that there is an additional symmetry constraint (cf. Table 3) that $m_5 + m_6 - n_5 - n_6$ must be even. Equivalently, states with even values of $\hat{N} = \hat{v}_5 + \hat{v}_6$ cannot couple to states with odd values $\hat{N}$. Given our definition of the constant of motion $\hat{L}$ in eq 5, this constraint leads to an effective Hamiltonian where states with even values of $\hat{v}_3$ cannot couple to states with odd values of $\hat{v}_3$.

In the classical Hamiltonian this symmetry is observed in the coupling of eq 17, where there is always a factor of 2 in front of the ψ_3 term. Considering the periodic boundary conditions, i.e., return to the same point when the variable changes by 2π, this causes the discrete symmetry $\psi_3 \rightarrow \psi_3 + \pi$ of the Hamiltonian. Accordingly, the eigenfunctions only have contributions from basis functions where n_3 is either even or odd only; i.e., the eigenfunctions can be sorted into symmetric ones and antisymmetric ones with respect to this discrete symmetry. Further symmetries of **H**, which, however, are of no special interest in the following are a shift of any angle by 2π and a simultaneous replacement of all angles by their negatives. These two symmetries guarantee the periodicity of the system on the toroidal configuration space and the time reversal symmetry of the Hamiltonian system.

IV. Numerical Examples for Semiclassical Wave Functions

We give numerical examples for the polyad $K = 7$, $L = 14$, $M = 0$. It contains a total of 288 states, and within the polyad we enumerate the states according to increasing energy.

The structure of the eigenfunctions at the energetically upper end of the polyad is most simple. Therefore we start with a discussion of the uppermost state, i.e., state number 288 of the polyad $K = 7$, $L = 14$, $M = 0$. Its energy is 8217 cm^{-1}. The six parts of Figure 3 show density (magnitude squared) and phase of the semiclassical wave function in the three planes $\psi_3 = 0$, $\psi_2 = \pi$ and $\psi_1 = \pi$, respectively. We see immediately that the density is concentrated along the 1-dimensional organization center $\psi_1 = \psi_2 = \pi$. There are no nodal lines; therefore both transversal excitation numbers are zero. In addition, the phase advance along this fiber is zero; therefore the longitudinal excitation number is also zero. In this sense the highest state, i.e., state 288, is the ground state of the organizational fiber $\psi_1 = \psi_2 = \pi$.

We use the word fiber above as the idealized central element of the dynamics. The organization element is a periodic orbit and its surrounding. This surrounding might be a bundle of concentric tori in the case of a stable central periodic orbit or some bundle of chaotic trajectories that run parallel to the central periodic orbit on average in the case of an unstable central periodic orbit.

Now we discuss the type of motion that is represented by this organization center and the interpretation of the excitation numbers relative to it. Along this fiber the angle ψ_3 moves freely, whereas the two angles ψ_1 and ψ_2 are locked at the values π. Looking at eq 16 of the canonical transformations, we see that locking of ψ_1 to a constant value means that the original mode 6 is coupled to the beat between modes 1 and 5 or alternatively and equivalently mode 5 is coupled to the beat between modes 1 and 6. Along the same line of reasoning the locking of ψ_2 to a constant value means that the original mode 6 is coupled to the beat motion between modes 2 and 5 or alternatively the coupling of mode 2 to the beat between modes 5 and 6. The simultaneous lockings of ψ_1 and ψ_2 to constant values also imply a 2:1 frequency coupling of mode 6 to the beat between modes 1 and 2. Mode 3 always runs freely, and the longitudinal excitation number, the phase advance divided by 2π, is the excitation number of mode 3. The transverse

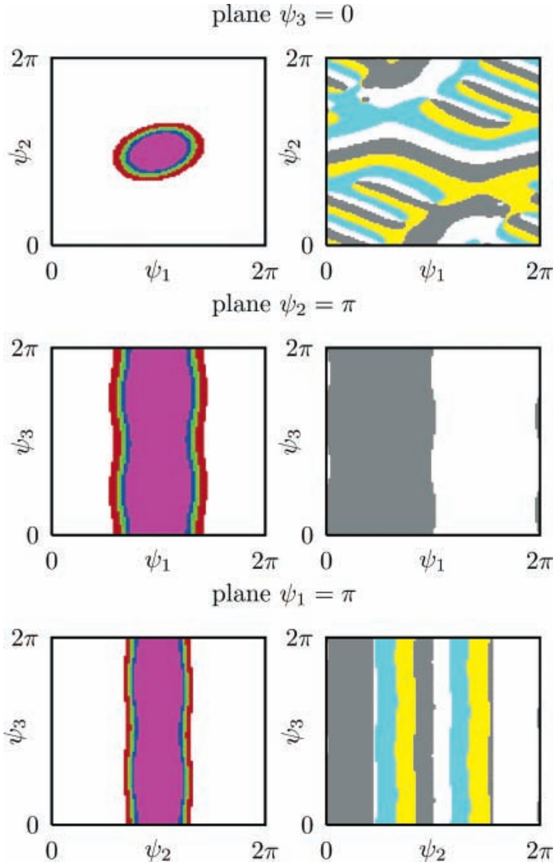

Figure 3. Semiclassical wave function of state 288 with energy 8217 cm^{-1}. Left panels show the density (magnitude squared) and right panels show the phase as functions of two coordinates indicated for a fixed value of the third coordinate. In density plots, density decreases from pink, blue, green, to red. In the phase plots, the colors change from white, light blue, yellow to gray as the phase increases in increment of $\pi/2$ from 0 to 2π. In all the plots opposite boundary points of the square have to be identified to convert the square into a 2-dimensional torus.

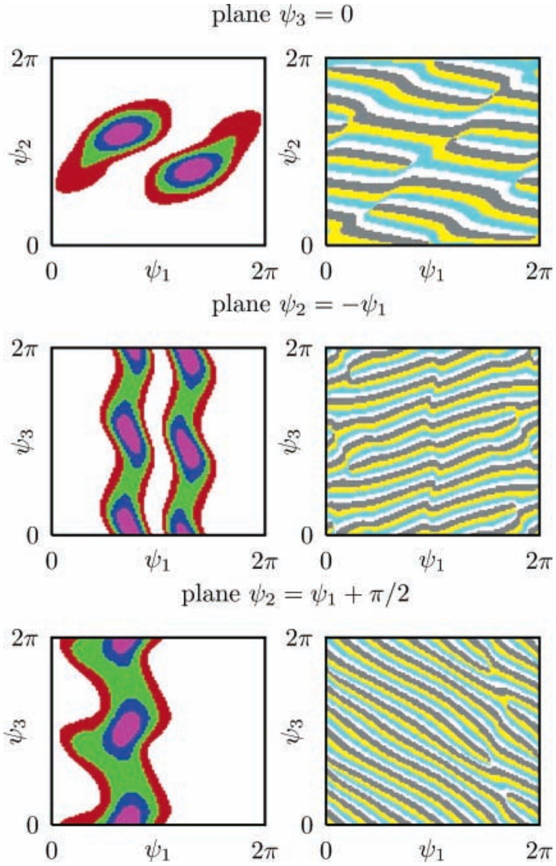

Figure 4. Slices of density (left) and phases (right) of the semiclassical wave function of state 96 with energy 7650 cm^{-1}. Otherwise the same as Figure 3.

excitation numbers indicate to which degree the couplings are out of phase or to which degree the motion fluctuates around the coupling point.

If we consider states at lower energy, then we encounter approximately 130 further states having various longitudinal and transversal excitation numbers organized around the same fiber. One of the lowest ones in energy of this group is state 96 at energy 7650 cm^{-1}. In Figure 4 we show density and phase of this state in the planes $\psi_3 = 0$, $\psi_2 = -\psi_1$ and $\psi_2 = \psi_1 + \pi/2$, respectively. From these plots it is evident that the transversal quantum number in the diagonal direction is $t_d = 0$, the transversal excitation number perpendicular to the diagonal is $t_p = 1$, and the longitudinal quantum number is $l = 9$. With such a high longitudinal excitation the fibers lead to some wiggles in ψ_1 and in ψ_2 directions and the density is no longer almost constant along the fibers. Nonetheless, fibers rotating around in ψ_3 directions stay clean. Note how the nodal plane is a plane of discontinuities of the phase.

If both transversal excitation numbers are large, then it becomes difficult to see a clean transverse structure because most of the density is pushed to the opposite sides of the torus, i.e., close to $\psi_1 = 0$ and/or to $\psi_2 = 0$. In particular, the fiber in the ψ_3 direction through $\psi_1 = 0$ and $\psi_2 = \pi$ seems to be the natural central fiber for a whole group of states in the middle of the polyad. In such cases it becomes more natural to count nodal lines from such opposite points. Incorporating this possibility into the scheme discussed so far adds approximately 30 further states clearly organized into fibers running in ψ_3 direction.

At the lower end of the polyad many states are organized around a different organizational element, namely, around the plane $\psi_2 = 0$. As a representative example we show in Figure 5 plots of the semiclassical wave function for state 10 at energy 7414 cm^{-1}. The various parts of the figure show density and phase in the planes $\psi_3 = 0$, $\psi_2 = 0$ and $\psi_1 = 0$, respectively. We see immediately how the density is concentrated around this organizatorial plane and that the phase function is simple in this plane only and has discontinuities outside. The singularities of the phase function become most evident in plane $\psi_1 = 0$; see part f of the figure. The transverse quantum number is $t = 0$; the two longitudinal quantum numbers are $l_1 = 0$ and $l_3 = 8$.

In the motion represented by this organization element the angles ψ_1 and ψ_3 move freely, whereas angle ψ_2 is locked to a constant value. As before, the locking of ψ_2 implies that in the original modes mode 6 is coupled to the beat between modes 2 and 5. Going up in energy, we find approximately 70 states organized around the same organizational element. In Figure 6 we present plots for state 132, which is one of the highest ones in this scheme at energy 7708 cm^{-1}. The various parts of the figure show density and phase in the planes $\psi_3 = 0$, $\psi_2 = \pi/5$ and $\psi_1 = \pi/4$, respectively. In this state there is a transverse excitation, and the plane $\psi_2 = 0$ itself is a nodal plane; therefore we show the plot in the parallel plane $\psi_2 = \pi/5$, which is a plane of high density. Note that the phase function in this plane of high density is a continuous deformation of a periodic plane wave whereas the phase function has singularities outside; see

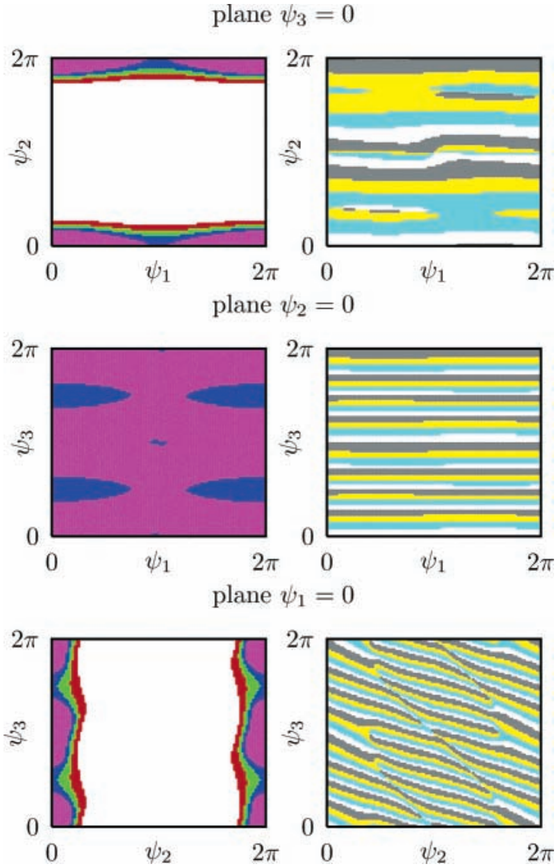

Figure 5. Slices of density (left) and phases (right) of the semiclassical wave function of state 10 with energy 7414 cm^{-1}. Otherwise the same as Figure 3.

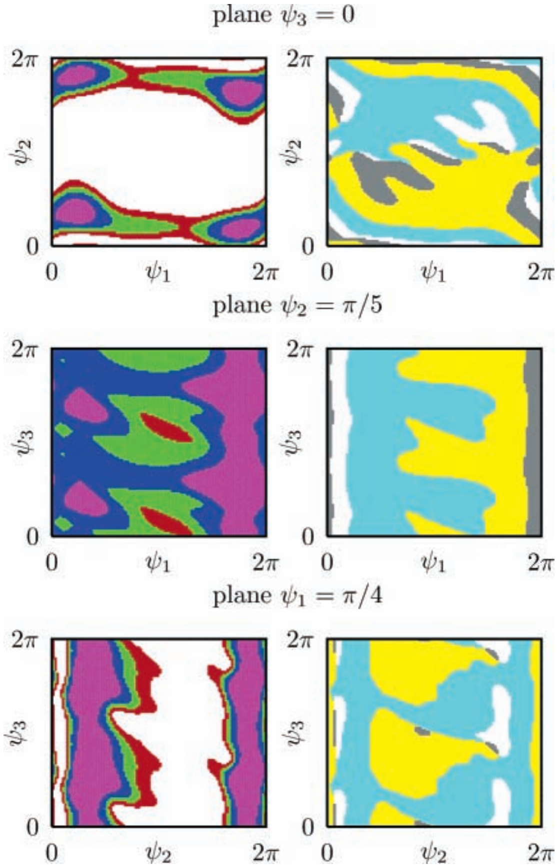

Figure 6. Slices of density (left) and phases (right) of the semiclassical wave function of state 132 with energy 7708 cm^{-1}. Otherwise the same as Figure 3.

parts d and f of the figure. From the plots we read off the quantum numbers $t = 1$, $l_1 = 1$ and $l_3 = 0$.

Going up in energy, the states show more and more variation of density inside of the plane ψ_2 = constant of high density. More and more fibers in ψ_3 direction appear, and accordingly, the other scheme discussed before becomes the more natural one to apply. Note that the energy of the state shown in Figure 6 is higher than the energy of the state shown in Figure 4. This demonstrates that the two ladders of states, discussed so far, interlace and make the total spectrum appear irregular and difficult to analyze even though most states belong to one of two rather simple and regular progressions of states.

In addition to these two long regular ladders of states, there are states that do not fall into these two schemes, this further increasing the complexity of the spectra. First there are states that show a regular, clean and simple structure of completely different type. To each one of such other organizational schemes, we could only find very few states. A good example is state 100 at energy 7654 cm^{-1} shown in Figure 7. The various parts of the figure show density and phase of the semiclassical wave function in the planes $\psi_3 = 0$, $\psi_2 = -\psi_1$ and $\psi_2 = \psi_1 + \pi$, respectively. The only plane in which we could find a rather clean and regular phase function is the plane $\psi_2 = \psi_1 + \pi$. In this plane we read off the longitudinal excitation numbers $l_1 + l_2 = 7$ and $l_3 = 8$. Note that because of mixing of basis functions only the combination $l_1 + l_2$ in the organization plane has a well-defined value whereas the excitation numbers l_1 and l_2 themselves do not have specific values. Seen from the plane $\psi_2 = \psi_1 + \pi$ the transverse excitation number is $t = 0$. This state does not fit well into any of the two schemes discussed above. There are a few more states with a similar density pattern but different longitudinal excitation numbers in the plane $\psi_2 = \psi_1 + \pi$. The phase coupling between the new angles ψ_1 and ψ_2 means for the original degrees of freedom a coupling of the degree of freedom 6 to half of the beat frequency between the degrees of freedom 1 and 2. There is also a small sequence of states with a clean and simple phase function in planes $\psi_1 = 0$.

Finally, there are states that look completely irregular. As a representative example we show state 98 at energy 7652 cm^{-1} in Figure 8. The various parts show density and phase in the planes $\psi_3 = 0$, $\psi_2 = 2\pi/5$, and $\psi_1 = 0$, respectively. In the density we do not recognize any clean nodal pattern and the phase function is not simple in any plane that could serve as a reasonable organizational center. Note that the phase has singularities also in the plane $\psi_2 = 2\pi/5$, which is the plane of highest density and which normally would be a natural candidate for an organizational structure. The phase is simple along some fibers in three directions but it is not evident what the transverse structure of these fibers is. This function seems to be a mixture of various patterns caused by state mixing because of near accidental degeneracy. There are many more similar cases, and some of such mixed states can be interpreted after demixing with the appropriate neighboring states.

Note how close in energy the states of Figures 4, 7, and 8 are. This demonstrates the interlacing of sequences belonging to different organizational patterns. Without a careful inspection of the wave functions a separation of the subsequences belonging to the various organizational structures is impossible, and we only recognize the irregular complete spectrum.

V. Conclusions

The complex eigenstate structure of SCCl$_2$ has been analyzed. Starting from the fitted potential of Strickler and Gruebele,[26]

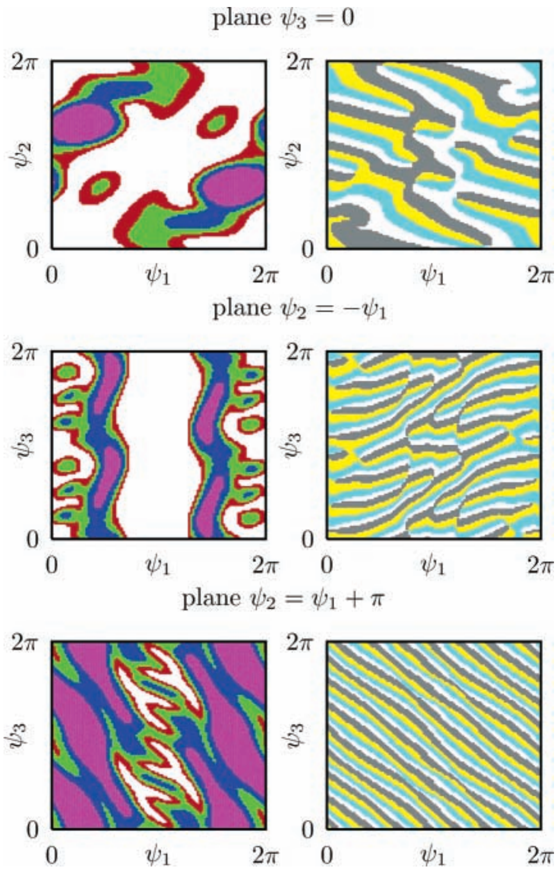

Figure 7. Slices of density (left) and phases (right) of the semiclassical wave function of state 100 at energy 7654 cm^{-1}. Otherwise the same as Figure 3.

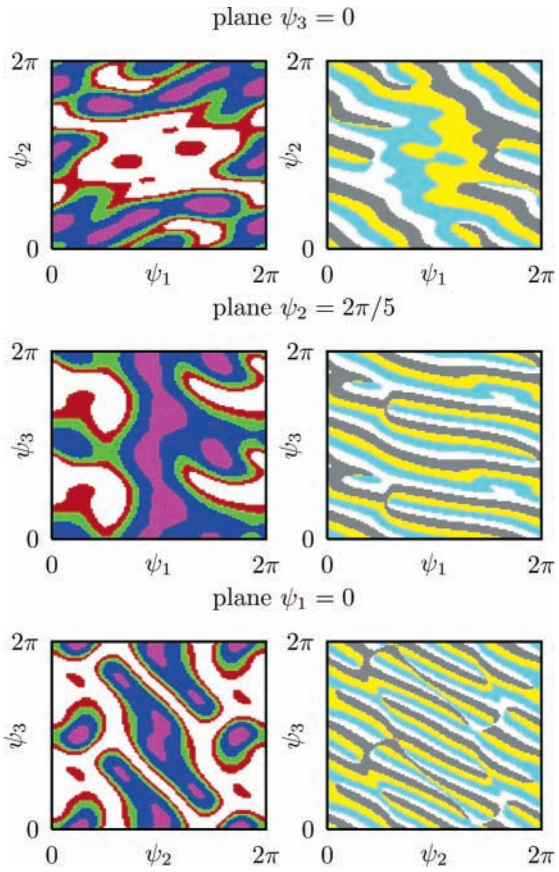

Figure 8. Slices of density (left) and phases (right) of the semiclassical wave function of state 98 at energy 7652 cm^{-1}. Otherwise the same as Figure 3.

the Van Vleck perturbation method was used to create a spectroscopic Hamiltonian and three polyad constants of the motion. Taking the classical limit and employing a canonical transformation, the number of the degrees of freedom was reduced to three, a number that allows for visual inspection of wave functions. In our chosen reduced configuration space angle variables we can infer whether particular classical motions become phase locked and hence semiclassical eigenfunctions to localize when the motion occupied a region of phase space where a particular resonance was active. This localization enabled the visual sorting of the eigenstates into ladders of states based on identified causal resonances. Assignment was carried out by counting nodes and phase advances associated with the density and phase of the eigenstate, respectively. For a large majority of states for which this was possible the three new values of nodal and angle quantum numbers plus the three polyad quantum numbers made up an assignment based on six approximate constants of the motion.

Two important long and several other short ladders of states were recognized and assigned. A generic drawing of the spinal organizing center (a torus of lower dimension, here a line and a plane) in each ladder about which the states of the ladder localize, was itself the most fundamental reduced dimension dynamic motion that the ladder states quantize. An approximate transformation can be made on this organization center to show it in the full six dimensions. Such a task is not rewarding as viewing anything in six dimensions presents problems.

A significant number of states, about 25%, did not fall on any ladders. Our experience is that many of these could be shown to be due to a quantum and/or classical mixing. The former occurs when several states on the same ladder are accidentally degenerate. The result are states with nearby energies that combine the original states linearly. As such, different linear combinations of these states can be made to show typical ladder type motions corresponding to missing rungs. Classical mixing is created when the flow seems to jump back and forth between two motions corresponding to two different resonant regions of phase space, i.e., between that of two ladders. We made no attempt here to carry out such steps in the analysis. There will also be some states so mixed up that it will be fruitless to do so.

The success of the analysis stems from five characteristics: (1) The qualitative insight of nonlinear dynamics. (2) The said conversion of the quantum problem in full dimension to a semiclassical one in reduced dimension by use of a canonical transform that takes advantage of the polyad and other constants of motion to remove cyclic angle coordinates. (3) The choice of the reduced angle variables to be sums of the full dimension angles configured to ensure that the former have zero velocity when the rational ratio resonance frequency condition is met. This leads to a predictable localization of those of the quantized, now semiclassical wave functions, which are affected by the particular resonance. In reverse, the localized appearance of the reduced dimension wave function reveals which resonances govern it and makes sorting simple. (4) The revealing use of plots of phase advances as well as the usual density. (5) The fact that the spectroscopic as opposed to the initial Hamiltonian contains only the most important interactions, leaving out those that are small, albeit trajectory and wave function disfiguring ones. This allows for the identification of the good, here polyad, constants of the motion, a problem unsolved for the initial Hamiltonian.

Acknowledgment. This work has been supported by CONACyT under grant number 33773-E, by DGAPA under grant number IN-118005, by the National Science Foundation under Grant No. 0315243 and by DOE under contract number DE-FG03-01IR15147.

References and Notes

(1) Bigwood, R.; Millan, B.; Gruebele, M. *Chem. Phys. Lett.* **1998**, *3*, *287*, 33.

(2) Herzberg, G. *Infrared and Raman Spectra of Polyatomic Molecules*; Van Norstrand Reinhold: New York, NY, 1945

(3) Keshavamurthy, S.; Ezra, G. S. *J. Chem. Phys.* **1997**, *107*, 156.

(4) Joyeux, M.; Sugny, D.; Lombardi, M.; Jost, R.; Schinke, R.; Skokov, S.; Bowman, J. *J. Chem. Phys.* **2000**, *113*, 9610.

(5) Joyeux, M.; Schinke, R.; Grebenshchikov, S. Y. *J. Chem. Phys.* **2004**, *120*, 7426.

(6) Joyeux, M.; Sugny, D.; Tyng, V.; Kellman, M. E.; H. I., Field, R. W.; Beck, C.; Schinke, R. *J. Chem. Phys.* **2000**, *112*, 4162.

(7) Kellman, M. E.; Dow, M. W.; Tyng, V. *J. Chem. Phys.* **2003**, *118*, 9519.

(8) Azzam, T.; Schinke, R.; Farantos, S. C.; Joyeux, M.; Peterson, K. A. *J. Chem. Phys.* **2003**, *118*, 9643.

(9) See, Gomez Llorente, J. M.; Pollak, E. *Annu. Rev. Phys. Chem.* **1992**, *43*, 91 and references therein. Farantos, S. C. *Int. Rev. Phys. Chem.* **1996**, *15*, 345.

(10) Borondo, F.; Vergini, E.; Wisniacki, D. A.; Zembekov, A. A.; Benito, R. M. *J. Chem. Phys.* **2005**, *122*, 111101.

(11) Kellman, M. E. *J. Chem. Phys.* **1990**, *93*, 6630.

(12) Kellman, M. E.; Chen, G. *J. Chem. Phys.* **1991**, *95*, 8671.

(13) Sibert, E. L.; McCoy, A. B. *J. Chem. Phys.* **1996**, *105*, 469.

(14) Jacobson, M. P.; Jung, C.; Taylor, H. S.; Field, R. W. *J. Chem. Phys.* **1999**, *111*, 600. Jung, C.; Taylor, H. S.; Jacobson, M. P. *J. Phys. Chem. A* **2001**, *105*, 681.

(15) McCoy, A. B.; Sibert, E. L. *J. Chem. Phys.* **1990**, *92*, 1893.

(16) Chirikov, B. V. *Phys. Rep.* **1979**, *52*, 26.

(17) Nielsen, H. H. *Rev. Mod. Phys.* **1951**, *23*, 90.

(18) Sibert, E. L. *J. Chem. Phys.* **1988**, *88*, 4378.

(19) Sibert, E. L. *Comput. Phys. Commun.* **1988**, *51*, 149.

(20) Zuñiga, J.; Bastida, A.; Requena, A.; Sibert, E. L. *J. Chem. Phys.* **2002**, *116*, 7495.

(21) Jung, C.; Ziemniak, E. M.; Taylor, H. S. *J. Chem. Phys.* **2001**, *115*, 2499.

(22) Waalkens, H.; Jung, C.; Taylor, H. S. *J. Phys. Chem. A* **2002**, *106*, 911.

(23) Jung, C.; Taylor, H. S.; Atilgan, E. *J. Phys. Chem. A* **2002**, *106*, 3092.

(24) Jung, C.; Mejia-Monasterio, C.; Taylor, H. S. *J. Chem. Phys.* **2004**, *120*, 4194.

(25) Jung, C.; Mejia-Monasterio, C.; Taylor, H. S. *Phys. Chem. Chem. Phys.* **2004**, *6*, 3069.

(26) Strickler, B.; Gruebele, M. *Phys. Chem. Chem. Phys.* **2004**, *6*, 3786.

(27) Heisenberg, W. *Z. Phys.* **1925**, *33*, 879.